Empirical Dynamic Modeling for Low-Altitude UAV Propagation Channels

Huang, Zeyu ; Rodrıguez-Pineiro, Jose; Domınguez-Bolano, Tomas; Cai, Xuesong; Yin, Xuefeng

Published in:
IEEE Transactions on Wireless Communications

DOI (link to publication from Publisher):
10.1109/TWC.2021.3065959

Publication date:
2021

Document Version
Accepted author manuscript, peer reviewed version

Empirical Dynamic Modeling for Low-Altitude UAV Propagation Channels

Zeyu Huang, José Rodríguez-Piñeiro, Tomás Domínguez-Bolaño, Xuesong Cai, *Member, IEEE* and Xuefeng Yin, *Member, IEEE*

***Abstract*—During the last few years, with the decrease of their sizes and costs, Unmanned Aerial Vehicles (UAVs) became more feasible for their use in general-purpose applications. As an important basis for UAV applications, the Air-to-Ground (A2G) radio propagation channel has gained attention in the channel modeling literature. However, whereas the A2G propagation channel is inherently dynamic (time-varying), the majority of the available models do not consider such a time-variability. In this paper, a dynamic stochastic channel model for A2G communications in realistic suburban scenarios is proposed. The model is able to stochastically characterize parameters related to the birth and time-of-life of the multi-path components (MPCs), as well as their evolution in terms of delay, Doppler frequency or magnitude. Correlation coefficients to relate different channel characteristics are also obtained. Our work shows that the MPCs evolution over time for the UAV A2G channel can be described by simple regular patterns.**

***Index Terms*—Air-to-ground, MPCs tracking, time-variant channel, UAV-based measurement.**

I. Introduction

Recently, low altitude Unmanned Aerial Vehicles (UAVs) have attracted much attention due to their extensive applications, such as monitoring of gas pipelines, forest inventory or logistics service [1]–[3]. More specifically, UAVs are supposed to have a significant role in the Fifth Generation Communication Systems (5G), in applications such as substituting a Base Station (BS) after communication infrastructure damage due to natural disasters, performing as a moving BS in temporary crowded areas or play the role of communications relay in some special circumstances as described in [4]–[7]. Hence, the design of UAV-based communication systems has become more and more important. One of the most important links in an UAV communication system is the Air-to-Ground (A2G) one (understood as a bi-directional channel, with both uplink and downlink communications). The most common A2G communication is between the UAV and a terrestrial BS. In order to optimize and evaluate the performance of A2G communication systems, it is essential to understand the A2G propagation channel. Accurate measurement-based channel models are necessary in order to perform cost-efficient communications performance evaluations based on simulations [8]. Many results were already proposed in literature, such as in [9]–[19]. In these papers, stochastic models for the path loss, shadowing, delay spread and other propagation channel characteristics are proposed.

However, due to the inherent mobility of UAVs, the A2G propagation channel for UAVs is time-variant. In time-variant channels, the multi-path components (MPCs) for different time instants are not independent and their evolution defines the so-called "trajectories" in delay, power or Doppler frequency domains (e.g., see [14]–[16], [19]–[22]).). In other words, when we represent the evolution of the delay, power or Doppler frequency of the MPCs with respect to the time or position of the UAV, some sort of lines or other geometrical patterns arise, which are commonly named trajectories. This evolution of the MPCs can be used to define an effective time-variant channel model. For example, in [20] a trajectory-based channel model has been proposed for a subway-to-infrastructure communication system.

In order to develop such trajectory-based channel models, the variation of the MPCs needs to be accurately described first. In [23], recursive Expectation-maximization (EM) and Space-Alternating Generalized Expectation-maximization (SAGE)-inspired High-Resolution Parameter Estimation (HRPE) algorithms were proposed to trace the evolution of the Direction Of Arrival (DOA). In [24]–[26] the Kalman filtering and extended Kalman filtering have been used to track the MPC parameters variation. Particle filter-based methods have also been used to identify the MPCs variation in [27], [28] and [29]. Recently, also some cluster-based studies have been proposed in [30], [31]. In this kind of method, it is often required to use K-means or Density-based Spatial Clustering of Applications with Noise (DBSCAN) algorithms to initialize several centroids of MPC clusters. Other alternatives are based on the application of image processing techniques to detect patterns in power delay

Z. Huang is with the College of Electronics and Information Engineering, Tongji University, Shanghai, China, and also with the CD-Lab for Dependable Wireless Connectivity, Institute of Telecommunications, TU Wien, Vienna, Austria. (e-mail: huangzeyu@tongji.edu.cn, zeyu.huang@tuwien.ac.at).

J. Rodríguez-Piñeiro and X. Yin are with the College of Electronics and Information Engineering, Tongji University, Shanghai, China. (e-mail: j.rpineiro@tongji.edu.cn and yinxuefeng@tongji.edu.cn).

T. Domínguez-Bolaño is with the CITIC Research Center & Department of Computer Engineering, University of A Coruña, A Coruña, Spain. (e-mail: tomas.bolano@udc.es).

X. Cai is with the Wireless Communication Networks Section, Department of Electronic Systems, Aalborg University, Aalborg, Denmark. (e-mail: xuc@es.aau.dk).

Corresponding author: José Rodríguez-Piñeiro (e-mail address: j.rpineiro@tongji.edu.cn).

This work was supported by the National Natural Science Foundation of China (NSFC) under Grants 61850410529 and 61971313; as well as by the Xunta de Galicia (by grant ED431C 2020/15, and grant ED431G2019/01 to support the Centro de Investigación de Galicia "CITIC"), the Agencia Estatal de Investigación of Spain (by grants RED2018-102668-T and PID2019-104958RB-C42) and ERDF funds of the EU (FEDER Galicia 2014-2020 & AEI/FEDER Programs, UE). The financial support by the Austrian Federal Ministry for Digital and Economic Affairs and the National Foundation for Research, Technology and Development is gratefully acknowledged.

profile (PDP) representations, such as [32].

The characteristics of the UAV A2G links, due to the relative "clearance" of the channel (in general, not many elements around the UAV disturb the propagation during the flight), can lead to very long and overlapping trajectories, since the reflections caused by the ground environment elements are usually not blocked for long distances [19]. Moreover, with the fast variation of the channel parameters, there are cases in which these trajectories can merge or diverge between them. These characteristics can make the majority of the aforementioned methods fail on tracking the MPCs. In this paper, a new MPC tracking algorithm, featuring a low computational complexity, is proposed and its effectiveness is supported by extensive simulations . Based on the detected trajectories, a dynamic A2G propagation channel model for UAVs is proposed. The results for 8 different height values ranging from $15\,\mathrm{m}$ to $105\,\mathrm{m}$ and UAV-BS distances between $50\,\mathrm{m}$ and $500\,\mathrm{m}$ were analyzed , which ensures the broad applicability of the proposed model.

The main works and contributions of this paper are: *a)* A multipath component distance (MCD)-based tracking algorithm with relatively low complexity is proposed to identify the multiple MPC-trajectories observed in the channel. The effectiveness of the tracking algorithm is verified via extensive simulations. The identified time-varying trajectories allow us to well establish the dynamic channel model; and *b)* Based on empirical MPC-trajectory tracking results for actual measurements in suburban environments, a dynamic stochastic channel model for A2G low-altitude UAV communications is established, which includes the "birth-death" behaviors of the trajectories, etc. To our best knowledge, this model is the first of its kind in characterizing the time-varying radio propagation channel between a low-altitude UAV and a terrestrial BS.

The structure of the rest paper is as follows: Section II presents the performed measurement campaign, including the measurement system and the measurement environment. In Section III, the proposed tracking algorithm is introduced and verified via extensive simulations. The dynamic channel model is investigated comprehensively detail in Section IV. Important findings are revisited and discussed in Section V. Concluding remarks are finally included in Section VI.

II. Measurement Setup and Scenario

In this paper, the signals acquired in the measurement campaign described in our previous work [19] were used. All the details of the measurement equipment and scenarios are included in that work, and hence the reader is referred to that paper for detailed explanations. However, for the sake of completeness, the basic aspects are introduced in this section as well. Section II-A describes the measurement system and configuration. Section II-B includes the details of the measurement scenario.

A. Measurement System and Configuration

Fig. 1a shows the block diagram of the measurement system and Figs. 1b to 1d pictures of it. The two topmost blocks of the block diagram, labeled as "Air Part", represent the measurement system mounted on the UAV itself (see a picture of it in Fig. 1b). The green block at the left of "Air Part" contains the hardware to acquire the signals, whereas the blue block at the right is used to control the reception and store the acquired signals. The bottom-most blocks, labeled as "Ground Part", represent the measurement system at the ground (see a picture of it in Fig. 1c). The left block of "Ground Part" contains the hardware required to transmit the signals, whereas the blue block at the right side is used to control the transmission and has stored the transmit signals. During the measurements, the ground part equipment was placed on a lift whose height was fixed at about $15\,\mathrm{m}$ (see Fig. 1d). For convenience, in this paper we refer to the ground part as BS.

Parameter	Value
sampling frequency	15.36 MSamples/s (upsampled to 25 MSamples/s when transmitting)
FFT size	1024 points
used subcarriers	600 (excluding DC)
effective used bandwidth	9 MHz
subcarrier spacing	15 kHz
cyclic prefix length	72 samples

TABLE I: Parameters of the OFDM transmit signal.

Both the air and the ground parts make use of Universal software Radio Peripherals (USRPs) N-210 from Ettus Research to receive and transmit the signals, and both the UAV and the BS are equipped with identical omnidirectional antennas. Furthermore, it is worth noting that the transmitter and receiver are time-synchronized by means of Global Positioning System (GPS)-disciplined clocks and the position of the UAV is real-time tracked based on the GPS estimates. This also enables to compensate the effect of the radiation pattern of both the transmitter and receive antennas by taking into account the relative position and orientation of the UAV and of the BS. The instantaneous positioning information of the UAV is estimated by decoding the National Marine Electronics Association (NMEA) strings captured by the GPS-disciplined clock onboard the UAV. In order to minimize the effect of the estimation noise in the positioning information, and taking advantage of the fact that the flight routes are defined as straight lines, a linear robust regression method [33] was applied to obtain a better estimation of the flight trajectory by using all the individual estimated UAV coordinates for the whole flight. It is expected that the errors in the positioning estimation are almost negligible. The two control blocks in Fig. 1a communicate with each other by using a standard Wi-Fi connection, allowing to start/stop the reception at the air node from the ground equipment (only when the UAV flies close to the BS, due to the limited coverage radio of the Wi-Fi link).

The "GTEC 5G Simulator" [34]–[37] was used to generate the transmit signals as well as to process the acquired data to obtain the channel impluse response. The "GTEC 5G Simulator" is a versatile piece of software that enables to fully configure the transmit signal and includes all the necessary developments for processing the acquired samples,

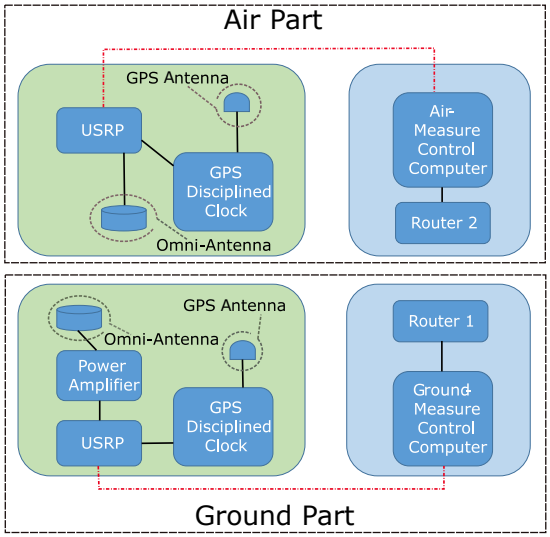

(a) Block diagram of the measurement system. The blocks labelled by "air part" are installed in the UAV, whereas the ones labeled as "ground part" are static in a lift of about 15 m height.

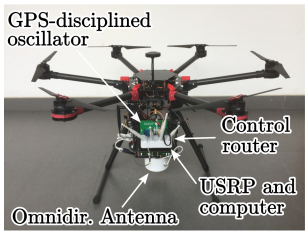

(b) Picture of the air part.

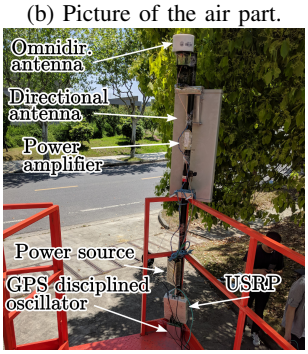

(c) Details of the ground part.

(d) Picture of the ground part.

Fig. 1: Considered measurement equipment.

such as channel estimation, interpolation and equalization algorithms, as well as time and frequency synchronization[1]. In this case an orthogonal frequency-division multiplexing (OFDM) signal following a frame structure similar to that defined by the 10 MHz downlink profile of long-time-evolution (LTE) [38] was considered, being the base sampling frequency 15.36 Msamples/s, the total used bandwidth 9 MHz and the carrier frequency 2.5 GHz, which does not conflict with the Wi-Fi communications adopted for control purposes, in the 2.4 GHz band. The main parameters of the considered signal

[1]The source code of both the GTEC Testbed and the GTEC 5G Simulator is publicly available under the GPLv3 license at https://bitbucket.org/tomas_bolano/gtec_testbed_public.git.

Fig. 2: Measurement environment.

are shown in Table I.

B. Measurement Environment and Scenarios

The measurement environment can be characterized as time-variant[2]. The measurements were conducted at the Jiading Campus of Tongji University, imaged in Fig. 2. In Fig. 2, the position of the BS is highlighted and the dashed line represents the flying route of the UAV during the measurements. The starting and end points of the UAV flights are also marked. The environment is a suburban scenario consisting of low- and middle-height buildings, open grass areas, trees, roads and lakes. Around the air route there are several buildings. The building labeled as "Building A", close to the starting point of the air route, has a height slightly lower than 15 m, whereas the Building B is approximately 63 m height. Close to the end point there is we can find the Building C, being about 25 m height.

Eight different height values were considered for the UAV flights, which are 15 m, 25 m, 35 m, 45 m, 60 m, 75 m, 90 m and 105 m. The choice of the flight altitude range is based on the legal regulations of the scenario under consideration. Moreover, the altitude range fits well with the regulations in many countries for commercial applications using small-sized UAVs [9]. The speed of the UAV was approximately 5 m/s. The propagation conditions can be characterized as possibly obstructed Line-of-Sight (LoS). More specifically, the LoS component can be partially obstructed for the lowest flight, i.e. the one at 15 m height, whereas we can expect LoS conditions for the rest.

III. Multi-Path Components Tracking Algorithm

In this section, a low-complexity channel MPC tracking algorithm is proposed. The proposed algorithm has been used to analyze actual data collected in a measurement campaign. Firstly, Section III-A will give insights in the basics of the

[2]In our measurement scenario, there are very few cars or other moving elements in the environment. Furthermore, the flight trajectory is far away from crowded roads and crosses an area with mostly static ground elements. Hence, the "time variability" is expected to be mainly caused by the movement of the UAV itself.

acquired data processing and formally introduce the concept of MPC trajectory. Then, in Section III-B, we will define the MCD[33] and introduce the way of calculating it, whereas Section III-C will detail the proposed MCD-based MPC tracking algorithm. Finally, Section III-D analyzes the performance of the proposed algorithm based on simulations.

A. MPC Trajectories Identification

The "GTEC 5G Simulator" receiver includes an implementation of the well-known SAGE algorithm [39] used to estimate a number of parameters of the MPCs from the acquired signal samples. During the UAV flight, we transmit a set of OFDM frames, each lasting 1 ms. The variation of the channel within the duration of an OFDM frame is negligible and hence we will consider all the parameters of each MPC static during such a time period. We consider the signal samples of an OFDM frame to estimate the "instantaneous" channel parameters. Those "instantaneous" parameters obtained from the signal samples corresponding to an OFDM frame will be referred as a snapshot. 10 captured channel impluse responses (CIRs) are considered for each snapshot to avoid spurious MPCs. The CIR model for the x-th snapshot is written as

$$h(t_x, \tau) = \sum_{l=1}^{L(x)} \alpha_{x,l} \delta(\tau - \tau_{x,l}) \exp\{j2\pi\nu_{x,l} t\}. \quad (1)$$

In (1), t_x is the time instant of the x-th snapshot, τ represents the propagation delay, $\alpha_{x,l}$, $\tau_{x,l}$ and $\nu_{x,l}$ are respectively the complex amplitude, delay and Doppler frequency of the l-th path at the x-th snapshot, $\delta(\cdot)$ denotes the impulse function (Dirac delta), and $L(x)$ is the number of estimated paths, which can be different for different snapshots. The estimated MPCs per snapshot will be ordered by increasing delay value, i.e.,

$$\tau_{x,l_1} > \tau_{x,l_2}, \forall l_1 > l_2. \quad (2)$$

The total number of snapshots is X. From the estimated MPCs, we are able to obtain the PDP of the channels. From the estimates of the MPCs parameters we can reconstruct the estimated delay-Doppler joint power spectrum and compare it with the measured one. Note that in the SAGE estimation, the model order selection, i.e., selecting the proper path number $L(x)$, is crucial to obtain realistic estimation results. In this work, we exploit the Akaike information criterion (AIC) principle [40], [41] for this purpose. Specifically, we first calculate the noise floor which is estimated by adding 3 dB to the mean power of the tail samples in the raw PDP. For each snapshot, the SAGE algorithm is first applied with a large number of paths (15 paths) to pre-estimate the MPC parameters, then we mark the path number that is larger than noise floor per snapshot. Finally, the SAGE algorithm is applied again with the path number that we marked to extract the MPC components. It is important to mention that, even for the obstructed LoS cases, the power of the lowest-delay MPC is always noticeably larger than that of the others for each snapshot. Hence, the lowest-delay MPC for each snapshot will be regarded as the LoS MPC.

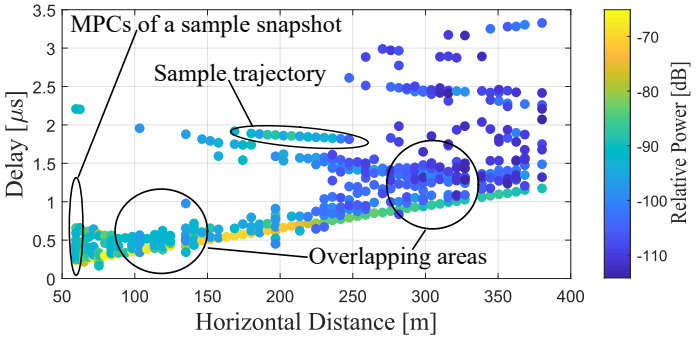

Fig. 3: Estimated Power Delay Profile, being the flight height 15 m.

Fig. 3 shows the delay estimates of the extracted MPCs versus the so-called horizontal distance between the BS and the UAV for flight height equal to 15 m. We refer as "horizontal distance" to the projection of the distance between the UAV and the BS on the ground, i.e., the difference of height is not considered. This is a convenient way to compare the results for different flight heights among them: if for two flights at different heights the value of horizontal distance for a snapshot is equivalent, we can conclude that the UAV is at the same position in both flights, except for the height component. Each dot in the figure corresponds to a MPC and its color codes the relative power. The x-axis is the horizontal distance between the BS (acting as a transmitter) the UAV (acting as a receiver) and the y-axis the MPC delay. The MPCs belonging to a sample snapshot are enclosed with an ellipse for illustration purposes. Basically, all the $L = 15$ points in the figure for a specific horizontal distance value correspond to a single snapshot.

When the UAV moves, the parameters (power, delay and Doppler frequency) of the MPCs change from one snapshot to another. In some cases it is intuitive to find a relationship between a MPC in a snapshot and another MPC in the next snapshot. Hence, we can understand them as a single MPC that evolves with time from one snapshot to another. The MPC variation trajectory, hereinafter referred as trajectory, can be viewed as the variation of the parameters of a certain MPC with the UAV movement. A sample trajectory was marked in Fig. 3, which shows that the concept of trajectory can have a clear geometrical interpretation in the PDP results, since the delay was observed to be the a quite coherent parameter with the UAV flight. The trajectories could also be plot as the variation of the Doppler frequency of the MPCs in the Doppler Power Spectral Density, but the delay was considered for the representations since the other MPC parameters change less smoothly over distance. As an example, Fig. 5a shows the variation of the power for the MPCs labeled as "sample trajectory" in Fig. 3 and Fig. 5b shows the variation in Doppler frequency. It can be seen how the fluctuations of the power are much less regular than those of the delay. The fluctuations of the Doppler frequency are not as drastic those of the power, but still much less smooth than those of the delay. However, when looking for a method to gather together MPCs into trajectories, the information provided by a single parameter

(e.g., the delay) may not be enough, specially when there could be many different MPC candidates to be included in a single trajectory, as can happen in areas where many MPCs are very close or almost overlap in terms of delay, such as those marked in Fig. 3. Hence, no matter how the trajectories are represented, it is important to understand that they are defined as the variation of the MPCs as a whole, i.e., including all their parameters.

It must be noted that, although the transmitted OFDM frames have silence periods between them, by means of the SAGE algorithm together with the channel model shown in (1) we are able to estimate the channel even in the silence periods. This allows us to obtain a channel estimation for the whole UAV trajectory, namely $h(t,\tau)$. We can then obtain easily the coherence time of the channels, which is a parameter of interest for our analysis. For that we calculate the correlation of the channel, namely $R_H(t,\Delta t)$, considering for each t a window of 10 s of $h(t,\tau)$. Then the coherence time is obtained as:

$$T_{\text{coh}} = \frac{1}{2}\left(\underset{\Delta t>0}{\arg\min}\left(\frac{|R_H(t,\Delta t)|}{R_H(t,0)}=0.5\right) - \underset{\Delta t<0}{\arg\min}\left(\frac{|R_H(t,\Delta t)|}{R_H(t,0)}=0.5\right)\right). \tag{3}$$

The obtained coherence times of the channel impulse responses for the different flight altitudes are shown in Fig. 4. Several statistical parameters of interest about the coherence time are also shown in Table II. As expected, because the UAV is moving at a slow speed (5 m/s), the coherence time is significatively large, with a mean value larger 100 ms and with maximum values larger than 300 ms for some cases.

In the next section we define the concept of MCD as a measure of the difference between two MPCs from different snapshots, which will be a tool to decide if they can belong to a common trajectory or not.

B. Multipath Component Distance

We use the MCD [42] to evaluate the difference between MPCs of different snapshots. Let x and y be snapshot indexes, with $x \neq y$, and i and j refer to the number of path within a snapshot. Hence, let $\text{MPC}_{x,i}$ denote the i-th MPC of the x-th snapshot and $\text{MPC}_{y,j}$ the j-th MPC of the y-th snapshot. The MCD between the $\text{MPC}_{x,i}$ and $\text{MPC}_{y,j}$ is

$$\text{MCD}_{x,i,y,j} = \sqrt{a\Delta^2\tau_{x,i,y,j} + b\Delta^2\nu_{x,i,y,j} + c\Delta^2 p_{x,i,y,j}}. \tag{4}$$

In (4), a, b and c are weighting variables. The definitions of $\Delta\tau_{x,i,y,j}$, $\Delta\nu_{x,i,y,j}$ and $\Delta p_{x,i,y,j}$ are respectively as follows:

$$\Delta\tau_{x,i,y,j} = |\tau_{x,i} - \tau_{y,j}| \tag{5}$$

$$\Delta\nu_{x,i,y,j} = |\nu_{x,i} - \nu_{y,j}| \tag{6}$$

$$\Delta p_{x,i,y,j} = |p_{x,i} - p_{y,j}|, \tag{7}$$

being $\tau_{x,i}$, $\nu_{x,i}$ and $p_{x,i}$ are the estimated delay, Doppler and relative power in dB of $\text{MPC}_{x,i}$. $p_{x,i}$ can be calculated as

$$p_{x,i} = 20\log_{10}|\alpha_{x,i}|, \tag{8}$$

where $\alpha_{x,i}$ is the estimated complex amplitude of $\text{MPC}_{x,i}$.

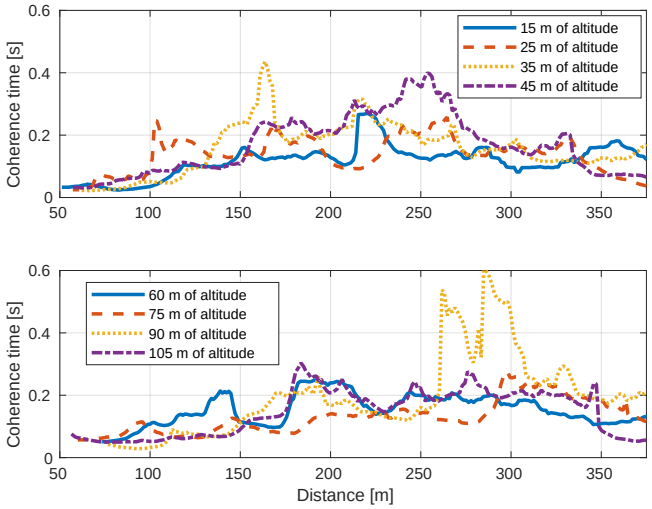

Fig. 4: Coherence times.

altitude	mean	std. deviation	minimum	maximum
15 m	0.1028	0.0559	0.01598	0.2697
25 m	0.1124	0.0684	0.01397	0.2577
35 m	0.1382	0.0918	0.01299	0.4356
45 m	0.1493	0.1006	0.01499	0.3986
60 m	0.1362	0.0628	0.01399	0.2498
75 m	0.1112	0.0618	0.01499	0.2757
90 m	0.1595	0.1322	0.01299	0.6094
105 m	0.1320	0.0766	0.01798	0.3037

TABLE II: Statistical parameters (in seconds) of the coherence times.

C. MPC Trajectories Tracking Algorithm

In order to extract the trajectories from the estimated PDP, We propose a MCD-based tracking algorithm. The tracking algorithm considers two steps:

1) **Parameters Initialization**: In our proposal, if the MCD of two MPCs from consecutive snapshots is less than a threshold value, namely T, these two MPCs will be considered as belonging to the same trajectory. However, in order to perform the analysis, we firstly need to choose proper values for T, as well as for the weighting parameters a, b and c of (3). We choose the trajectory formed by the LoS MPCs to set our parameters. Let $\tau^i_{LoS}, i = 1\ldots I$ denote the delay value of the i-th LoS MPC, where I is the total number of the LoS MPCs. Hence, we define $\Delta\tau^i_{LoS}$, $i = 1\ldots I-1$ as

$$\Delta\tau^i_{LoS} = \tau^{i+1}_{LoS} - \tau^i_{LoS}, \tag{9}$$

being both $\Delta\nu^i_{LoS}$ and Δp^i_{LoS} defined analogously. The weighting parameters a, b and c in the MCD calculation are respectively defined as

$$a = 1/\text{SD}\left(\Delta\tau^i_{LoS}\right) \tag{10}$$

$$b = 1/\text{SD}\left(\Delta\nu^i_{LoS}\right) \tag{11}$$

$$c = 1/\text{SD}\left(\Delta p^i_{LoS}\right), \tag{12}$$

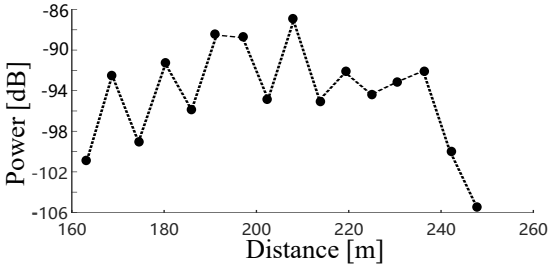

(a) Power fluctuation of the trajectory labeled as "Sample trajectory" in Fig. 3. Each point corresponds to a MPC. It can be seen that the variation in power is not as smooth and monotonic as that of delay.

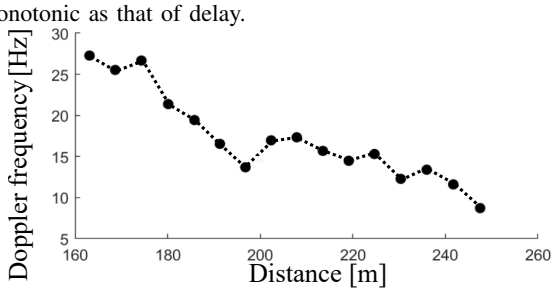

(b) Doppler frequency fluctuation of the trajectory labeled as "Sample trajectory" in Fig. 3. Each point corresponds to a MPC. It can be seen that the variation in Doppler frequency is not as smooth and monotonic as that of delay.

Fig. 5: Power and Doppler frequency fluctuations for the MPCs of the trajectory labeled as "Sample trajectory" in Fig. 3.

where $\mathrm{SD}(\cdot)$ is the unbiased sample standard deviation, defined for $\Delta \mathrm{x}^i_{LoS}$, being x one of $\{\tau, \nu, p\}$, as

$$\mathrm{SD}\left(\Delta \mathrm{x}^i_{LoS}\right) = \sqrt{\frac{1}{I-2}\sum_{i=1}^{I-1}\left(\Delta \mathrm{x}^i_{LoS} - \frac{\sum_{i=1}^{I-1}\Delta \mathrm{x}^i_{LoS}}{I-1}\right)^2}. \tag{13}$$

Then, based on the previous definitions, the MCD between the i-th and $i+1$-th LoS MPC is

$$\mathrm{MCD}_{i,i+1} = \sqrt{a\Delta^2\tau^i_{LoS} + b\Delta^2\nu^i_{LoS} + c\Delta^2 p^i_{LoS}}, \tag{14}$$

with $i = 1 \ldots I-1$, and the threshold T is set as

$$T = \max(\mathrm{MCD}_{i,i+1}), \quad i = 1 \ldots I-1. \tag{15}$$

2) **Trajectories Tracking**: After the parameters are set, we trace the trajectories by means of the processing detailed in Flow-chart 2 (Fig. 6).

The two specified steps make use of a common module aimed to track a single trajectory starting at a given MPC or, in other words, infer the evolution on time of a given MPC. This process is described in Flow-chart 3 (Fig. 7).

D. Performance Verification

For testing the performance of the tracking algorithm we have introduced Monte-Carlo simulations with random realizations of propagation scenarios [43]. In these simulations we consider several scatterers along a straight flight route, with random distances between them and random perpendicular

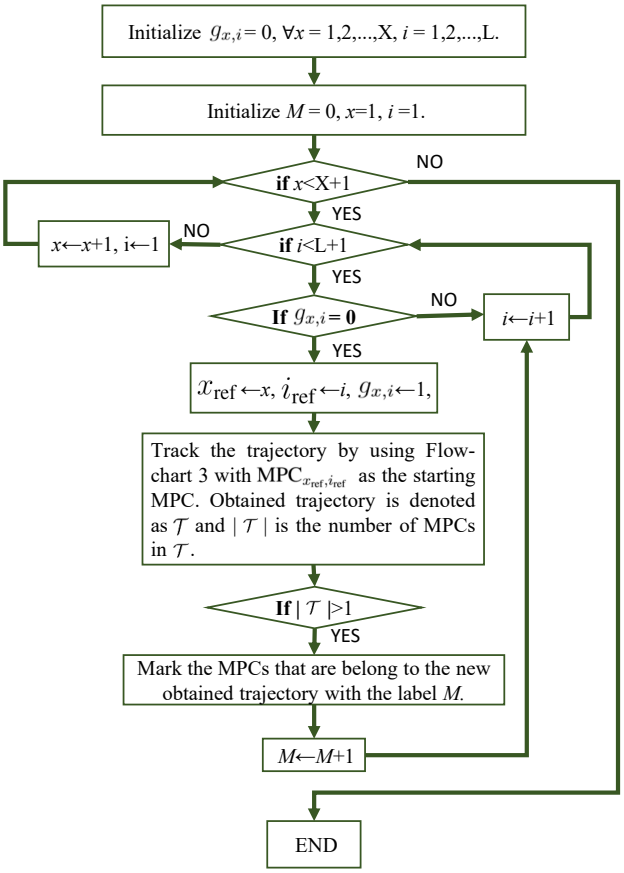

Fig. 6: Flow-chart 2 (Trajectories tracking). $g_{x,i}$ denotes if the MPC$_{x,i}$ was already processed by algorithm. If $g_{x,i} = 0$, MPC$_{x,i}$ was not processed yet. If $g_{x,i} = 1$, MPC$_{x,i}$ was processed already. M denotes the current trajectory index.

distances to the flight route. The received MPCs are then obtained from the reflections of the transmitted signal caused by these scatterers, where their power is calculated with the Friis transmission equation. Moreover, we consider that with some probability the scattering order (SO) may be larger than 1, i.e., the signal may be reflected by more than one scatterer before reaching the receiver. In the simulations, the generated scatterers are always "last hop" scatterers (i.e., the last scatterer in which the signal is reflected before reaching the receiver), and we model the case of SOs larger than one by adding an additional random delay and power loss to the received MPCs. Finally, we also consider that each scatterer may experience blockages (which will block completely the MPCs) randomly appearing along the flight and with a random duration. Table III shows the parameters of the statistical distributions used in the simulations. For each generated PDP in the simulations, a trajectory is randomly chosen to set the tracking parameters of the algorithm (with the method explained before). To evaluate the performance of the algorithm we define the miss-leading probability parameter ($\mathrm{P}_{\text{miss-leading}}$). For two consecutive MPCs belonging to the same trajectory, $\mathrm{P}_{\text{miss-leading}}$ is the probability that the MCD between these two MPCs is larger than the threshold. After executing our trajectory tracking algorithm over 100 channel realizations

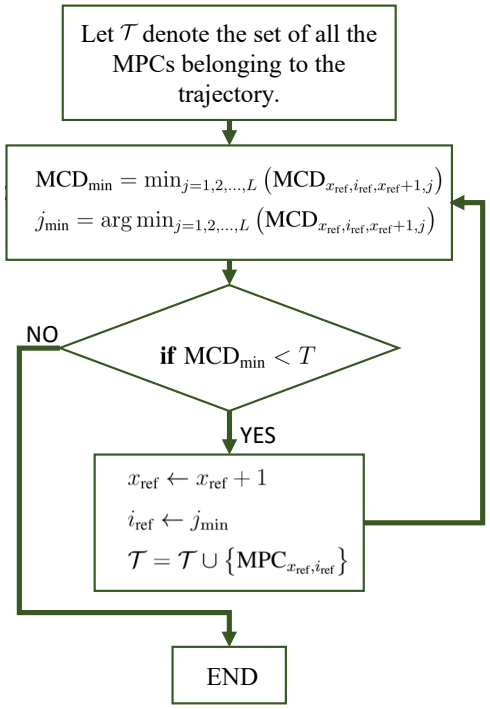

Fig. 7: Flow-chart 3 (Single trajectory tracking).

we have obtained an average $\text{P}_{\text{miss-leading}} = 0.0509$, with 95% confidence intervals of [0.0335 0.0680]. Hence, our algorithm is able to effectively track the MPCs trajectories exhibiting a high level of accuracy.

IV. Statistical Characteristics of Trajectories

In this section we present stochastic models to characterize the random behavior of the time-variant MPCs in the A2G propagation channel.

In order to obtain the stochastic models for the MPCs evolution, we applied the MPC tracking method to the data acquired in all the flights. Table IV shows the tracking parameters obtained for all the flight heights in our scenario. There is not an obvious relationship between the values of the parameters w.r.t. the flight height. Once the parameters have been set, the results obtained by the trajectory tracking algorithm for the 15 m flight height are shown in Fig. 8. The x-axis corresponds to the horizontal distance between the UAV and the BS and the y-axis corresponds to the MPCs delay. All the MPCs are shown as colored dots, being the color defined by their relative power. We connect dots belonging to the same trajectory by line segments (different colors are used for different trajectories).

The obtained trajectories can be divided into two different types: Line-of-Sight trajectories (LoSTs) and Non-Line-of-Sight trajectories (NLoSTs). All the MPCs in LoSTs are LoS components. On the contrary, each NLoST is formed by Non-Line-of-Sight (NLoS) paths. The NLoSTs are mainly caused by reflections and diffraction from the ground elements in the measurement environment. Since the MPC with the lowest delay per snapshot corresponds to a LoS MPC (see Section III-A) and the MPCs are ordered by increasing delay

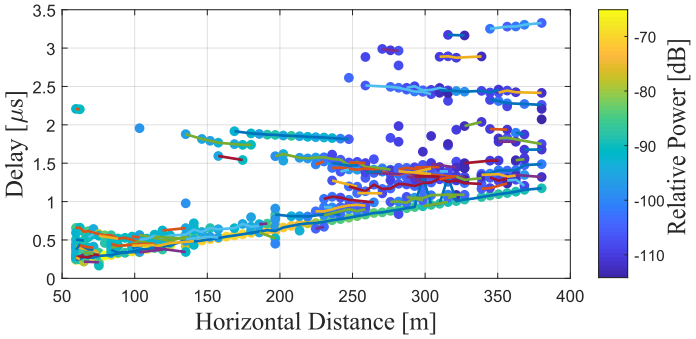

Fig. 8: Trajectories obtained by the MPCs tracking algorithm.

for each snapshot, if the parameters are appropriately set, the first detected trajectory, namely q_0, will be always a LoST. All the other detected trajectories, i.e., $\text{q}_1, \text{q}_2, \ldots, \text{q}_{Q-1}$, will be NLoSTs, where Q is the total number of obtained trajectories. Finally, note that the MPCs in Flow-chart 2 (Fig. 6) are ordered by increasing horizontal distance between the BS and the UAV. Hence, the algorithm will consider first the MPCs corresponding to low distances between the BS and the UAV and then those with larger distances. Hence, the tracked trajectories will be also ordered by the increasing horizontal distance of their starting points. Due to the LoS paths are determined by the positions of the BS and the UAV and the NLoS paths are always randomly generated during the flight of the UAV, the delay value of the LoS paths is more predictable. Therefore, the evolution of the LoST is more predictable than that of the NLoSTs. In this paper, we statistically characterize the NLoSTs with their relative variation w.r.t the LoST.

Several statistical characteristics for the different trajectories are proposed. For each of them, the basic concepts are firstly explained and then the stochastic models are presented with respect to the flight height. In order to validate the proposed models, the Kolmogorov-Smirnov testing (K-S testing) was used to investigate whether the empirical one-dimensional probability distributions can be described by a reference probability distribution [44]. Let denote $F_m(z)$ as the measured empirical Cumulative Distribution Function (CDF) of the random variable z, whereas $F_f(z)$ is the fitting CDF of $F_m(z)$ by using a reference distribution with known analytical expressions. The critical value D_{stat} is defined as

$$D_{\text{stat}} = \max\{|F_m(z) - F_f(z)|\}. \tag{16}$$

We define the null hypothesis as follows: $F_m(z)$ can be obtained from the reference probability distribution $F_f(z)$. The null hypothesis is rejected at level α if

$$D_{\text{stat}} > c(\alpha)\sqrt{\frac{A+B}{AB}}, \tag{17}$$

where A and B are the number of fitting and measured samples, respectively, and

$$c(\alpha) = -\sqrt{\frac{1}{2}\ln\alpha}. \tag{18}$$

The level α is the probability of committing a type I error, i.e., rejecting the null hypothesis (conclude that $F_m(z)$ does not follow the distribution $F_f(z)$) when it is actually true [44].

Value	Distribution	Parameters
Distance between consecutive scatterers	Exponential	$\lambda = 100\,\text{m}$
Distance from scatterers to flight route	Truncated Gaussian	$\mu = 75\,\text{m}$, $\sigma = 15\,\text{m}$, $[a, b] = [25, 300]\,\text{m}$
Scatterers height	Uniform	$[a, b] = [15, 90]\,\text{m}$
Scattering order (SO) > 1	Bernoulli	$p = 0.3$
Additional delay for SO > 1	Truncated Gaussian	$\mu = 0.75\,\mu\text{s}$, $\sigma = 0.5\,\mu\text{s}$, $[a, b] = [0.25, 2]\,\mu\text{s}$
Power loss coefficient for SO > 1	Uniform	$[a, b] = [0.5, 0.7]\,\mu\text{s}$
Distance between consecutive blockages	Exponential	$\lambda = 200\,\text{m}$
Length of blockages	Exponential	$\lambda = 100\,\text{m}$

TABLE III: Parameters of the statistical distributions used in the simulations.

Height [m]	a	b	c	T
15	96.937	1.074	0.823	8.472
25	87.545	0.496	0.393	6.770
35	93.648	0.715	0.313	6.260
45	73.620	0.627	0.854	5.523
60	80.161	0.781	0.114	7.135
75	107.116	0.749	0.128	7.158
90	111.825	1.077	0.093	5.999
105	79.637	0.606	0.556	8.068

TABLE IV: Obtained tracking algorithm parameters.

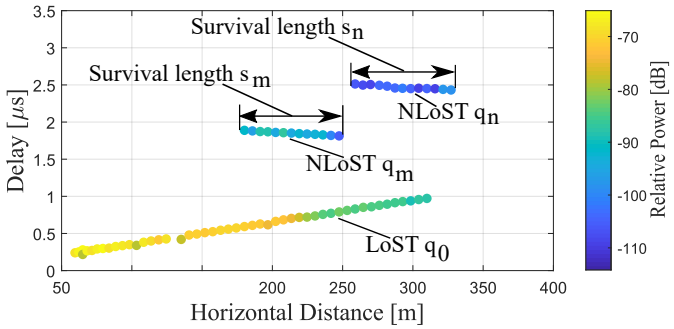

(a) Definition of survival length.

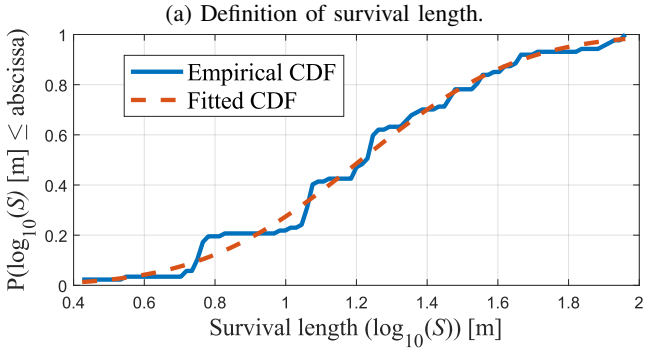

(b) Empirical and fitted CDFs for the 15 m-height flight.

Fig. 9: Sample results of the survival length.

The studied characteristics are as follows: in Section IV-A we define and statistically study the so-called survival length. The characteristics of the birth of NLoSTs w.r.t the movement of UAV are studied in Section IV-B. Modeling of the starting point of the NLoSTs can be found in Section IV-C. In Section IV-D we study the initial relative delay between the LoST and the NLoSTs. Section IV-E studies the number of trajectories along the flight and its dependence with the flight height. Section IV-F gives the correlation coefficients between the different statistical parameters extracted for the trajectories.

A. Survival Length of the NLoSTs

The survival length of a NLoST, namely s_q, where $q = 1, 2, \ldots, Q-1$, is used to describe how long each trajectory is visible in the PDP results. In this paper, the survival length for each NLoST is defined as follows: the absolute change in the horizontal distance between the UAV and the BS from the birth to the death of a trajectory[3]. In other words, the survival length for each NLoST will be the length of its projection onto the horizontal axis of the PDP. Fig. 9a illustrates two different NLoSTs, namely q_m and q_n, and their corresponding survival lengths, s_m and s_n. Because the NLoSTs births and deaths are random events, the survival length of the NLoSTs per flight can be characterized as a random variable, denoted by S. Based on our study, the survival length per flight can be well fitted using log-normal distributions. The level α of K-S testing here is specified to be 0.025.

Fig. 9b shows the empirical CDF and the corresponding fitting CDF for a sample flight at a height of $15\,\text{m}$; the x-axis is the survival length in logarithmic scale. Table V reports the parameters of the Lognormal (μ, σ) fittings per flight, with μ and σ denoting the mean and the standard deviation, respectively. The maximum mean value is $1.37\ \log_{10}(\text{m})$ (at $25\,\text{m}$ flight height) and the minimum mean value is $1.19\ \log_{10}(\text{m})$ (at $75\,\text{m}$ flight height). However, the maximum standard deviation is $0.52\ \log_{10}(\text{m})$ (at $25\,\text{m}$ flight height) and the minimum standard deviation $0.29\ \log_{10}(\text{m})$ (at $15\,\text{m}$ flight height). From the results, there is not an obvious dependence between the average survival length values and the flight height. The standard deviation values are increased w.r.t. the altitude except for the $25\,\text{m}$ case, which is much higher than others. This kind of variation with the increase of altitude ca be interpreted as follows: one the one side, the UAV detects longer trajectories which could due to the reduction of the blockage by low-height elements (e.g., see [19]); on the other side, due to the attenuation due to the propagation, some trajectories are shorter than for low altitude cases. For the $25\,\text{m}$ altitude flight, the average value and the standard deviation are both the largest in our measurement, which means that the set of trajectories length obtained for this flight is very rich. This phenomenon may caused by the height of surrounding buildings, which can produce a large set of powerful trajectories with different lengths.

[3]Trajectory birth is defined as the instant where the trajectory starts, whereas death is the instant when it disappears.

Height [m]	15	25	35	45
μ [$\log_{10}$(m)]	1.213	1.285	1.287	1.364
σ [$\log_{10}$(m)]	0.356	0.558	0.286	0.469
Height [m]	60	75	90	105
μ [$\log_{10}$(m)]	1.261	1.059	1.139	1.143
σ [$\log_{10}$(m)]	0.542	0.292	0.273	0.298

TABLE V: Parameters of the Lognormal distributions used to describe the survival length.

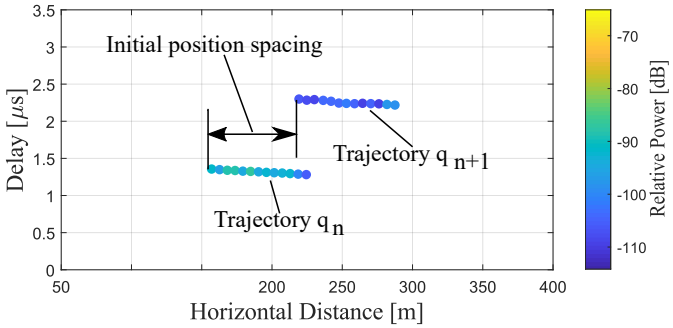

(a) Definition of initial position spacing.

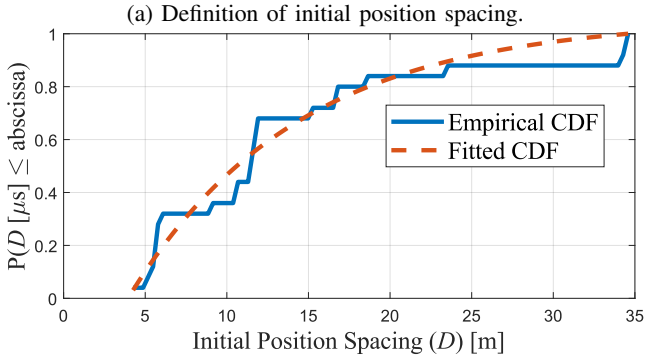

(b) Empirical and fitted CDFs for the 105 m-height flight.

Fig. 10: Sample results of initial position spacing.

Height [m]	15	25	35	45
λ	0.160	0.264	0.087	0.301
Height [m]	60	75	90	105
λ	0.306	0.282	0.072	0.097

TABLE VI: Parameters of the exponential distributions used to fit the initial position spacing.

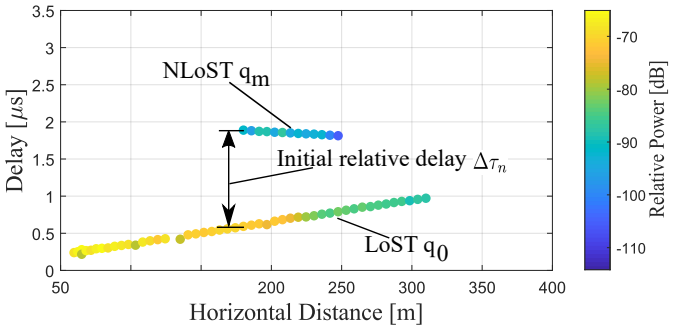

(a) Definition of initial relative delay.

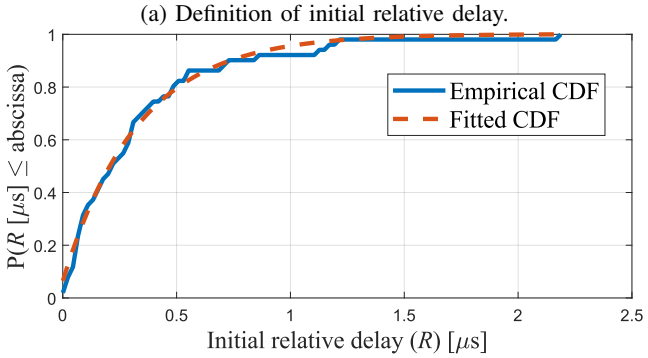

(b) Empirical and fitted CDF for the 60 m-height flight.

Fig. 11: Sample results of initial relative delay.

B. Initial Position Spacing

With the purpose of characterizing the birth of the NLoSTs during the flight of the UAV, we define the concept of initial position spacing. The initial position spacing is defined as the horizontal distance difference between the first MPCs of two consecutive trajectories. Here, the first MPC of each trajectory is that with the lowest BS-UAV horizontal distance. In Fig. 10a, the initial position spacing between two consecutive trajectories, namely q_n and q_{n+1}, is illustrated. The initial position spacing reflects the absolute value of the horizontal displacement of the UAV between the births of two consecutive trajectories.

The initial position spacings for a flight can be characterized by the random variable D. Fig. 10b plots the empirical CDF based on the measured data and the corresponding fitted CDF for the case in which the flight height is 105 m. We found out that these measured distributions can be fitted by exponential distributions, namely $E(\lambda)$. The level α of K-S testing here is 0.05 for all the flights. Table VI shows the obtained parameters for the exponential distributions of all flights. Note that if the initial position spacing follows an exponential distribution, the instant of appearance of new trajectories can be described as a Poisson stochastic process [45]. From the results, we can see that the largest average value for the exponential distribution, namely λ, corresponds to the 45 m flight. This means that, for this flight, the appearance rate new trajectories is higher than for the other flights. This is reasonable, since for the lowest altitude cases the appearance of new trajectories can be affected by the blockage from low-height architectural elements close to the fight route; whereas for the higher altitude flights the appearance of new trajectories can be impacted by the propagation attenuation.

C. Initial Relative Delay

For each NLoST, the initial relative delay is defined as the difference in delay between the first MPC of the NLoST and the MPC of the LoST for the same snapshot. The initial relative delay accounts for the difference in the propagation distance between the NLoS MPCs and the LoS ones. Fig. 11a illustrates the initial relative delay for a sample NLoST q_n, namely $\Delta\tau_n$.

The initial relative delay of the NLoSTs of a flight can be characterized by the random variable R. Fig. 11b shows the empirical CDF of the initial relative delay for the 60 m height

flight and the corresponding fitting. Exponential distributions $E(\lambda)$ can fit well the empirical CDF, being the level α of the K-S testing 0.05. Table VII provides the parameters of the fittings for all the flight heights. From the results shown in Table VII, no clear relationship between the flight altitude and the initial relative delay of the NLoST can be appreciated.

Height [μs]	15	25	35	45
λ	1.748	2.220	2.901	2.546
Height [μs]	60	75	90	105
λ	3.035	2.979	3.963	3.449

TABLE VII: Parameters of the exponential distributions used to fit the NLoSTs initial relative delay.

D. Linearized model for each NLoST

In this section, we firstly propose a linearized model (including two parameters), to fit the delay variation of each trajectory w.r.t. the horizontal distance between the UAV and BS. Secondly, based on the proposed model, the relative evolution of NLoSTs with respect to the LoST is characterized.

By establishing a trade-off between the accuracy of the results and the mathematical tractability of the proposed models, a straight line segment is used to model each detected trajectory. More specifically, the following linear model is proposed to describe the q-th trajectory:

$$\tau = k_q h + \beta_q, \tag{19}$$

where τ and h denote delay and horizontal distance, respectively, k_q and β_q are the slope and the intercept on delay axis of the q-th trajectory, respectively, and $q = 0, 1, \ldots, Q-1$, being Q the total number of detected trajectories. For each trajectory, we obtain the values of k_q and b_q by means of the least squares method. Fig. 12a shows the fitting results for all the detected trajectories, corresponding the dashed line to the LoST and the solid ones to the NLoSTs. For convenience, we use a different color to plot the fit of each trajectory.

For each MPC, we define the delay fluctuation, namely $\mathrm{f}_{x,i}$, as the delay difference from the corresponding fitting line to the MPC, where x is the snapshot index and i the number of MPC within the snapshot. We can characterize the delay fluctuation for the MPCs of a flight by the random variable F. The empirical CDF for a sample flight at 75 m height, obtained from the measured data, is shown in Fig. 12b, together with the proposed fit. Through K-S testing, we found that Normal (μ, σ) distributions fit well the delay fluctuation values, being the level α of the K-S test 0.025 in this case. Table VIII shows the value of the parameter σ of the Normal distributions for all the flights, being $\mu \approx 0$ in all the cases. From the Fig. 12b, we can observe that the delay fluctuation values gather around 0, and mainly in a reduced range approximately defined as $(-0.02, 0.02)\,\mu$s, which justifies the use of the linearized model. From the observed results, we can see that the delay fluctuation has no clear relationship with the flight altitude.

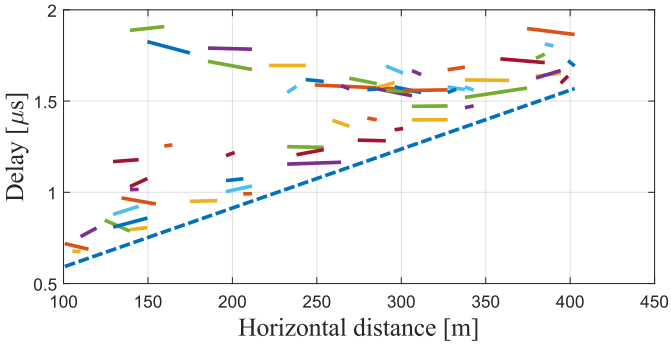

(a) Linear fits for the NLoSTs of 75 m flight.

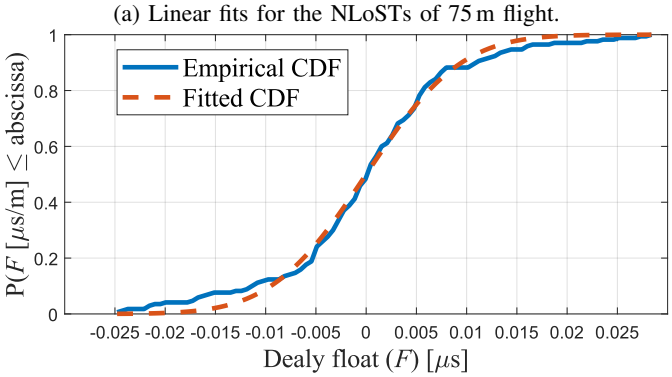

(b) Empirical and fitted CDF of the NLoST delay fluctuation for the 75 m-height.

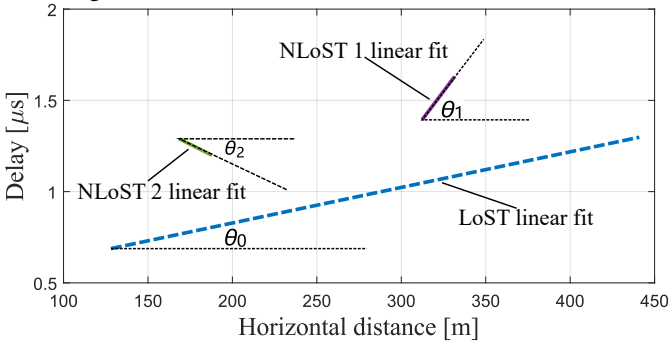

(c) Definition of the relative slope.

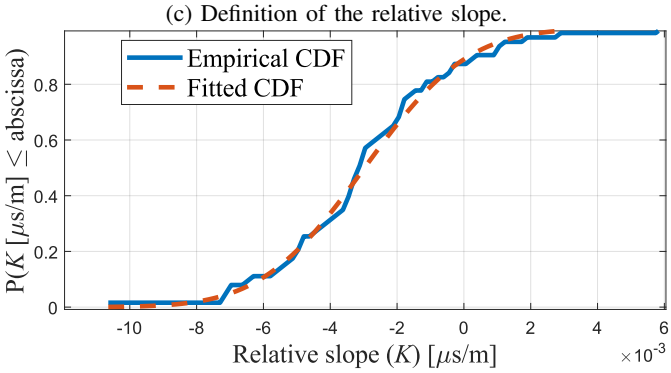

(d) Empirical and fitted CDF of the relative slopes of the NLoSTs for the 75 m height flight.

Fig. 12: Linearized model of the NLoSTs.

According to the model defined in (19), we use a straight line to fit each trajectory, being k_q its slope, with $q = 0, 1, \ldots, Q-1$. For each NLoST, we define the concept of relative slope with respect to the LoST, namely Δk_q, $q =$

Height [m]	15	25	35	45
σ [μs]	0.016	0.011	0.011	0.013
Height [m]	60	75	90	105
σ [μs]	0.016	0.007	0.010	0.012

TABLE VIII: Parameter σ of the Normal distributions used to fit the NLoST delay fluctuation. The value of the parameter μ is always zero.

$1, 2, \ldots, Q-1$, as follows:

$$\Delta k_q = \tan \Delta\theta_{\mathrm{r}}, \tag{20}$$

where

$$\Delta\theta_{\mathrm{r}} = \theta_{\mathrm{r}} - \theta_0, \text{ with}$$
$$\theta_{\mathrm{r}} = \arctan k_q, \text{ and}$$
$$\theta_0 = \arctan k_0, \text{ where}$$
$$\theta_{\mathrm{r}}, \theta_0 \in \left(-\pi/2,\, \pi/2\right).$$

From the definition above, the positive relative slope means that the corresponding NLoST gets further away from the LoST along with the increase of the horizontal distance between the BS and the UAV. An example of this is shown in Fig. 12c, labeled as "NLoST 1 linear fit". In Fig. 12c, θ_1 is greater than θ_0, hence the relative slope is positive. This also means that the propagation distance of the NLoS path that lead to the NLoST increases faster with the UAV movement than the propagation distance of the LoS path. On the contrary, negative relative slope means that the corresponding NLoST gets closer to the LoST with the increase of the horizontal distance. Hence, the propagation distance of the NLoS path that lead to the NLoST increases slower than that of the LoS path. In Fig. 12c, the line labelled as "NLoST 2 linear fit" shows an example of this situation. Since θ_2 is lower than θ_0, the relative slope is negative.

The relative slope of the NLoSTs per flight can be characterized by the random variable K. Fig. 12d shows the empirical CDF obtained from the measured data and the corresponding fitting CDF for a sample flight (45 m flight height). We use normal distributions $\mathcal{N}(\mu, \sigma)$ for the fittings, where μ denotes the mean and σ the standard deviation. The level α for the K-S testing is 0.025. Table IX shows the parameters of the fitting distributions for all the considered flight heights. The results show no noticeable dependency with the flight height. However, it can be pointed out that the average value for all the fittings is negative, which means that for all the cases the majority of NLoSTs get closer to the LoST with the increase of the horizontal distance.

E. Number of Simultaneous Trajectories

A parameter that can be used to intuitively show the dependence of the propagation characteristics with the flight height is the so-called "number of simultaneous trajectories", defined as the number of trajectories detected in each snapshot. In particular, Fig. 13 shows the the empirical CDF corresponding to the number of trajectories detected per snapshot. It has been found that a uniform distribution can fit the empirical CDF corresponding to each flight height, being the parameters of the respective uniform distributions detailed in Table X. It can be seen that, in general, the trend of the number of MPC trajectories is to decrease when the flight height increases. This is consistent with the intuition and findings in literature, i.e. the channel at a higher heights is more LoS-alike. However, it can also be appreciated that, for the extreme height cases (e.g., when the height is 105 m), the number of MPCs can slightly increase. This is also coherent with our findings for this measurement environment in [19], that also shows similar non-intuitive effects due to strong reflections from tall buildings, which are blocked by objects close to the UAV when the flight height is lower. For example, it was shown that increasing the flight height could lead to a decrease of the K-factor [19]. This indicates that there is a non-negligible dependence of the model with the flight height and that, although in general the channel becomes more LoS-alike when the flight height increases, sometimes the relationship between the number of trajectories and the flight height is not monotonic.

Height [m]	15	25	35	45
μ [μs/m]	-0.0032	-0.0031	-0.0031	-0.0028
σ [μs/m]	0.0030	0.0030	0.0025	0.0037
Height [m]	60	75	90	105
μ [μs/m]	-0.0022	-0.0030	-0.0015	-0.0037
σ [μs/m]	0.0028	0.0024	0.0016	0.0040

TABLE IX: Parameters of the Normal distributions used to fit the relative slopes of the NLoSTs

.

F. Relationship Between the Trajectories Characteristics

Up to this point, we have statistically characterized the general behavior of the trajectories. Whereas the initial position spacing is related with the rate of new trajectories birth, the survival length states how long they can last visible at the receiver. By means of the initial relative delay and the linear model for each trajectory, we can characterize how the variation of the NLoSTs is with respect to the LoST in each flight. In this section we study how the different parameters used to statistically describe the trajectories are related among them.

For each flight, many trajectories were obtained. For convenience, let us define three vectors as $\mathbf{s} = (s_1, s_2, \ldots, s_{Q-1})$, $\mathbf{\Delta\tau} = (\Delta\tau_1, \Delta\tau_2, \ldots, \Delta\tau_{Q-1})$, and $\mathbf{\Delta k} = (\Delta k_1, \Delta k_2, \ldots, \Delta k_{Q-1})$, where $Q-1$ is the number of NLoSTs. s_q, $\Delta\tau_q$ and Δk_q are the survival length, initial relative delay and relative slope of the q-th NLoST, respectively (see Sections IV-A, IV-C and IV-D). We define the correlation coefficient that describes the degree of linear correlation between the survival length and the relative slope, namely $r(S, K)$, as

$$r(S,K) = \frac{\sum_{q=1}^{Q-1}(s_q - \overline{\mathbf{s}})(\Delta k_q - \overline{\mathbf{\Delta k}})}{\sqrt{\sum_{q=1}^{Q-1}(s_q - \overline{\mathbf{s}})^2 \sum_{q=1}^{Q-1}(\Delta k_q - \overline{\mathbf{\Delta k}})^2}}, \tag{21}$$

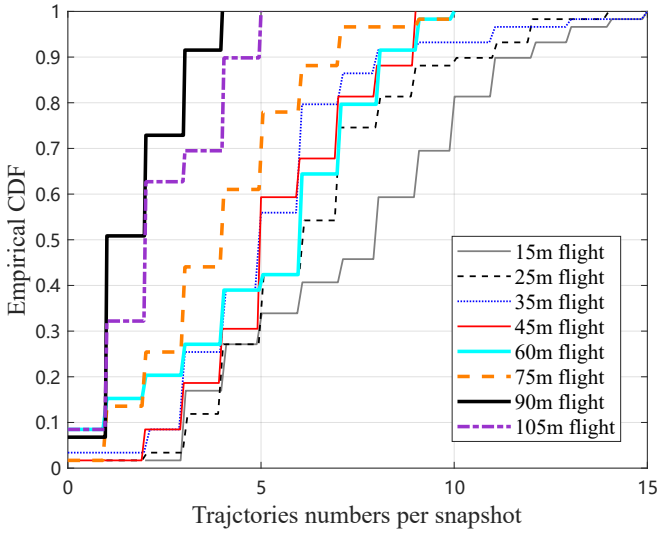

Fig. 13: Empirical CDF corresponding to the number of trajectories per snapshot.

Height [m]	15	25	35	45
a	1.071	1.665	0.597	1.712
b	13.214	11.047	10.013	9.136
Height [m]	60	75	90	105
a	0.371	0.314	0.011	0
b	9.900	7.619	3.684	4.984

TABLE X: Parameters of the uniform distributions corresponding to the number of trajectories per snapshot.

Height [m]	15	25	35	45
$r(S,K)$	0.187	0.204	0.066	0.122
$r(S,R)$	−0.060	0.111	−0.045	0.052
$r(K,R)$	−0.115	−0.012	−0.122	0.051
Height [m]	60	75	90	105
$r(S,K)$	0.253	0.324	0.467	0.124
$r(S,R)$	−0.013	−0.126	−0.205	0.245
$r(K,R)$	−0.145	−0.202	−0.178	−0.033

TABLE XI: Correlation coefficients for all the detected trajectories.

where $\bar{\mathbf{s}}$ is the mean value of $\mathbf{s}$ and $\overline{\mathbf{\Delta k}}$ is the mean value of $\mathbf{\Delta k}$. We can define $r(S,R)$ and $r(K,R)$ in an analogous way.

Table XI provides the correlation coefficient results obtained for all the flights. This table shows that these trajectory attributes do not exhibit a clear linear relationship between them.

V. Important Finding Revisited

A number of characteristics have been used in this contribution for describing the evolution of the MPCs. In this section, we summarize the main obtained results.

The following characteristics have been considered: *a)* the survival length, which is used to describe the distance travelled by the UAV between the NLoSTs birth and death processes; *b)* the initial position spacing, which describes the horizontal distance travelled by the UAV between the births of two consecutive NLoSTs; *c)* the initial relative delay, which accounts for the difference in delay between the LoST and the starting point of each NLoST; *d)* a linearized model for each NLoST, which includes the relative slope with respect to the LoST and the fluctuation of the NLoST with respect to the linearized model. Finally, we have also calculated the correlation coefficients between the different properties previously mentioned, distinguishing between the results in which all the trajectories are included and those in which only the long ones are considered.

From our study, we found out that:

- Lognormal distributions fit well the empirical distribution of the survival length. This means that there are much more short trajectories than long ones for each flight. The long trajectories are mainly caused by buildings or other regular structures of the ground environment. The amount of this kind of Interacting Objects (IOs) is much less than that of irregular IOs leading to the short trajectories, such as cars or trees[4].
- Exponential distributions are adequate to model the initial relative delay, which describes the delay difference between the birth point of each NLoST to the LoST.
- The birth of NLoSTs can be modeled as a Poisson stochastic process.
- The relative slopes of the NLoSTs with respect to te LoSTs follow normal distributions. Furthermore, the distribution of the relative slopes of the long trajectories is much more concentrated (i.e., has lower standard deviation) than that of the short ones. This may also be explained using a similar reasoning as that for the survival length, i.e., the long trajectories are generated in a more regular fashion by large-sized IOs not easily blocked by other ground elements. This also causes that the correlation coefficient between the survival length and the relative slope of the long NLoSTs is noticeably increased for high flights, since in these flights the reflections caused by large-sized IOs are less likely to be blocked by small elements of the propagation environment.
- The delay fluctuation of the MPCs with respect to their corresponding fitting line can be modeled by a Normal distribution.
- Based on the correlation coefficient results, if we consider all the trajectories per flight, their different properties do not exhibit clear dependency between them.
- The flight height does not change noticeably the statistical characteristics of the evaluated properties.

For convenience, all the parameters of the proposed stochastic models are summarized in the Tables XII and XIII.

VI. Conclusions

In this paper, we study the propagation for Air-to-Ground (A2G) links corresponding to low-altitude Unmanned Aerial

[4]The trajectories caused by small-sized IOs in the ground environment can be easily blocked by other elements of the environment when the UAV moves. Hence, their survival length is reduced in general.

Parameter	Random variable	Distribution
Survival length	S	Lognormal
Initial position Spacing	D	Exponential
Initial relative delay	R	Normal
Delay fluctuation	F	Normal ($\mu = 0$)
Relative slope	K	Normal

TABLE XII: Proposed characteristics, the corresponding random variables and the distribution.

Height [m]		15	25	35	45
S	$\mu\,[\log_{10}(\mathrm{m})]$	1.213	1.285	1.287	1.364
	$\sigma\,[\log_{10}(\mathrm{m})]$	0.356	0.558	0.286	0.469
D	λ	0.160	0.264	0.087	0.301
R	λ	1.748	2.220	2.901	2.546
F	σ	0.016	0.011	0.011	0.013
K	$\mu\,[\mu\mathrm{s/m}]$	-0.0032	-0.0031	-0.0031	-0.0028
	$\sigma\,[\mu\mathrm{s/m}]$	0.0030	0.0030	0.0025	0.0037
$r(S,K)$		0.187	0.204	0.066	0.122
$r(S,R)$		-0.060	0.111	-0.045	0.052
$r(K,R)$		-0.115	-0.012	-0.122	0.051
Height [m]		60	75	90	105
S	$\mu\,[\log_{10}(\mathrm{m})]$	1.261	1.059	1.139	1.143
	$\sigma\,[\log_{10}(\mathrm{m})]$	0.542	0.292	0.273	0.298
D	λ	0.306	0.282	0.072	0.097
R	λ	3.035	2.979	3.963	3.449
F	σ	0.016	0.007	0.010	0.012
K	$\mu\,[\mu\mathrm{s/m}]$	-0.0022	-0.0030	-0.0015	-0.0037
	$\sigma\,[\mu\mathrm{s/m}]$	0.0028	0.0024	0.0016	0.0040
$r(S,K)$		0.253	0.324	0.467	0.124
$r(S,R)$		-0.013	-0.126	-0.205	0.245
$r(K,R)$		-0.145	-0.202	-0.178	-0.033

TABLE XIII: Parameters of all the statistical model in this paper.

Vehicles (UAVs) in suburban environments. The obtained results are realistic since they are based in a measurement campaign which systematically analyzed the propagation for 8 different flight heights.

Different from other works in the literature, in this paper we consider a time-variant approach to model the propagation between the terrestrial Base Station (BS) and the UAV. In order to do this, we firstly define the concept of "trajectory" of a multi-path component (MPC), which is used describe the evolution of such MPC with the UAV flight. We propose a multipath component distance (MCD)-based method to track the evolution of the MPCs with the UAV flight and hence obtain the MPC trajectories. We model each of them as a straight line segment, showing that this model describes well the trend of the MPCs evolution. Several properties, including the so-called survival length, initial position spacing, initial relative delay or relative slope were defined and statistically characterized for the trajectories in each flight. From those results, a stochastic model of the MPCs evolution for low-altitude UAV communications in suburban environments is developed, which leads to the basis of a time-varying radio propagation channel between a low-altitude UAV and a terrestrial BS.

The obtained results are able to effectively explain the underlying propagation mechanisms for different flight heights and are very valuable for the optimization of the network deployments as well as the transceivers for UAV-based applications. Furthermore, the consideration of time-varying channel models is essential to evaluate the effectiveness of A2G communication links to serve UAVs for services with different Quality-of-Service (QoS) requirements in a environment which is inherently changing with the movement of the UAV.

REFERENCES

[1] D. Hausamann, W. Zirnig, G. Schreier, and P. Strobl, "Monitoring of gas pipelines - a civil UAV application," *Aircraft Engineering and Aerospace Technology*, vol. 77, pp. 352–360, 10 2005.

[2] L. Wallace, A. Lucieer, C. Watson, and D. Turner, "Development of a UAV-LiDAR system with application to forest inventory," *Remote Sensing*, vol. 4, no. 6, pp. 1519–1543, 2012. [Online]. Available: http://www.mdpi.com/2072-4292/4/6/1519

[3] M. R. Haque, M. Muhammad, D. Swarnaker, and M. Arifuzzaman, "Autonomous quadcopter for product home delivery," in *2014 International Conference on Electrical Engineering and Information Communication Technology*, April 2014, pp. 1–5.

[4] H. Shakhatreh, A. H. Sawalmeh, A. Al-Fuqaha, Z. Dou, E. Almaita, I. Khalil, N. S. Othman, A. Khreishah, and M. Guizani, "Unmanned aerial vehicles (UAVs): A survey on civil applications and key research challenges," *IEEE Access*, vol. 7, pp. 48 572–48 634, 2019.

[5] Y. Zeng, R. Zhang, and T. J. Lim, "Wireless communications with unmanned aerial vehicles: opportunities and challenges," *IEEE Communications Magazine*, vol. 54, no. 5, pp. 36–42, May 2016.

[6] Z. Ma, B. Ai, R. He, G. Wang, Y. Niu, and Z. Zhong, "A wideband non-stationary air-to-air channel model for uav communications," *IEEE Transactions on Vehicular Technology*, vol. 69, no. 2, pp. 1214–1226, 2020.

[7] A. A. Khuwaja, Y. Chen, N. Zhao, M. Alouini, and P. Dobbins, "A survey of channel modeling for uav communications," *IEEE Communications Surveys Tutorials*, vol. 20, no. 4, pp. 2804–2821, 2018.

[8] Z. Huang, J. Rodríguez-Piñeiro, T. Domínguez-Bolaño, X. Yin, D. Matolak, and J. Lee, "Performance of 5G terrestrial network deployments for serving UAV communications," in *14th European Conference on Antennas and Propagation (EuCAP 2020)*, Copenhagen, Denmark, March 2020, pp. 1–5, special session "Propagation for Unmanned Aerial Vehicles (UAVs)". Online access: http://dx.doi.org/10.23919/EuCAP48036.2020.9135609.

[9] R. Amorim, H. Nguyen, P. Mogensen, I. Z. Kovács, J. Wigard, and T. B. Sørensen, "Radio channel modeling for UAV communication over cellular networks," *IEEE Wireless Communications Letters*, vol. 6, no. 4, pp. 514–517, Aug 2017.

[10] D. W. Matolak and R. Sun, "Air-ground channel characterization for unmanned aircraft systems – Part III: The suburban and near-urban environments," vol. 66, pp. 6607–6618, 2017.

[11] T. Tavares, P. Sebastiao, N. Souto, F. J. Velez, F. Cercas, M. Ribeiro, and A. Correia, "Generalized LUI propagation model for UAVs communications using terrestrial cellular networks," in *2015 IEEE 82nd Vehicular Technology Conference (VTC2015-Fall)*, Sep. 2015, pp. 1–6.

[12] X. Cai, A. Gonzalez-Plaza, D. Alonso, L. Zhang, C. B. Rodríguez, A. P. Yuste, and X. Yin, "Low altitude UAV propagation channel modelling," in *2017 11th European Conference on Antennas and Propagation (EUCAP)*, March 2017, pp. 1443–1447.

[13] X. Ye, X. Cai, X. Yin, J. Rodríguez-Piñeiro, L. Tian, and J. Dou, "Air-to-ground big-data-assisted channel modeling based on passive sounding in LTE networks," in *2017 IEEE Global Communications Conference (GLOBECOM 2017)*, Singapore, December 2017, pp. 1–6, workshop "Vehicular Communications based on 5G". Online access: http://dx.doi.org/10.1109/GLOCOMW.2017.8269204.

[14] X. Cai, N. Wang, J. Rodríguez-Piñeiro, X. Yin, A. Pérez-Yuste, W. Fan, G. Zhang, and G. F. Pedersen, "Low altitude air-to-ground channel characterization in LTE network," in *13th European Conference on Antennas and Propagation (EuCAP 2019)*, Krakow, Poland, March-April 2019, pp. 1–5.

[15] N. Wang, X. Yin, X. Cai, J. Rodríguez-Piñeiro, and A. P. Yuste, "A novel air-to-ground channel modeling method based on graph model," in *13th European Conference on Antennas and Propagation (EuCAP 2019)*, Krakow, Poland, March-April 2019, pp. 1–5.

[16] X. Cai, J. Rodríguez-Piñeiro, X. Yin, N. Wang, B. Ai, G. F. Pedersen, and A. P. Yuste, "An empirical air-to-ground channel model based on passive measurements in LTE," *IEEE Transactions on Vehicular*

Technology, vol. 68, no. 2, pp. 1140–1154, 2019, online access: http://dx.doi.org/10.1109/TVT.2018.2886961.

[17] K. Tu, J. Rodríguez-Piñeiro, X. Yin, and L. Tian, "Low altitude air-to-ground channel modelling based on measurements in a suburban environment," in *11th International Conference on Wireless Communications and Signal Processing (WCSP 2019)*, Xi'an, China, October 2019, online access: http://dx.doi.org/10.1109/WCSP.2019.8927975.

[18] X. Cai, C. Zhang, J. Rodríguez-Piñeiro, X. Yin, W. Fan, and G. F. Pedersen, "Interference modeling for low-height air-to-ground channels in live LTE networks," *IEEE Antennas and Wireless Propagation Letters*, vol. 18, no. 10, pp. 2011–2015, August 2019, online access: http://dx.doi.org/10.1109/LAWP.2019.2936264.

[19] J. Rodríguez-Piñeiro, T. Domínguez-Bolaño, X. Cai, Z. Huang, and X. Yin, "Air-to-ground channel characterization for low-height UAVs in realistic network deployments," *IEEE Transactions on Antennas and Propagation*, vol. 69, no. 2, August 2020, online access: http://dx.doi.org/10.1109/TAP.2020.3016164.

[20] X. Cai, X. Yin, X. Cheng, and A. P. Yuste, "An empirical random-cluster model for subway channels based on passive measurements in UMTS," *IEEE Transactions on Communications*, vol. 64, no. 8, pp. 3563–3575, Aug 2016.

[21] R. He, C. Schneider, B. Ai, G. Wang, Z. Zhong, D. A. Dupleich, R. S. Thomae, M. Boban, J. Luo, and Y. Zhang, "Propagation channels of 5g millimeter-wave vehicle-to-vehicle communications: Recent advances and future challenges," *IEEE Vehicular Technology Magazine*, vol. 15, no. 1, pp. 16–26, 2020.

[22] R. He, B. Ai, G. L. Stüber, G. Wang, and Z. Zhong, "Geometrical-based modeling for millimeter-wave mimo mobile-to-mobile channels," *IEEE Transactions on Vehicular Technology*, vol. 67, no. 4, pp. 2848–2863, 2018.

[23] P.-J. Chung and J. Bohme, "Recursive EM and SAGE-inspired algorithms with application to DOA estimation," *IEEE Transactions on Signal Processing*, vol. 53, no. 8, pp. 2664–2677, 2005.

[24] A. Richter, J. Salmi, and V. Koivunen, "An algorithm for estimation and tracking of distributed diffuse scattering in mobile radio channels," in *2006 IEEE 7th Workshop on Signal Processing Advances in Wireless Communications*, July 2006, pp. 1–5.

[25] W. Wang, T. Jost, and A. Dammann, "Estimation and modelling of NLoS time-variant multipath for localization channel model in mobile radios," in *2010 IEEE Global Telecommunications Conference GLOBECOM 2010*, Dec 2010, pp. 1–6.

[26] M. Zhu, J. Vieira, Y. Kuang, K. Åström, A. F. Molisch, and F. Tufvesson, "Tracking and positioning using phase information from estimated multi-path components," in *2015 IEEE International Conference on Communication Workshop (ICCW)*, June 2015, pp. 712–717.

[27] X. Yin, G. Steinbock, G. E. Kirkelund, T. Pedersen, P. Blattnig, A. Jaquier, and B. H. Fleury, "Tracking of time-variant radio propagation paths using particle filtering," in *2008 IEEE International Conference on Communications*, May 2008, pp. 920–924.

[28] M. Froehle, P. Meissner, and K. Witrisal, "Tracking of UWB multipath components using probability hypothesis density filters," in *2012 IEEE International Conference on Ultra-Wideband*, Sep. 2012, pp. 306–310.

[29] K. Saito, K. Kitao, T. Imai, and Y. Okumura, "Dynamic MIMO channel modeling in urban environment using particle filtering," in *2013 7th European Conference on Antennas and Propagation (EuCAP)*, April 2013, pp. 980–984.

[30] Q. Wang, B. Ai, R. He, K. Guan, Y. Li, Z. Zhong, and G. Shi, "A framework of automatic clustering and tracking for time-variant multipath components," *IEEE Communications Letters*, vol. 21, no. 4, pp. 953–956, April 2017.

[31] C. Huang, A. F. Molisch, Y. Geng, R. He, B. Ai, and Z. Zhong, "Trajectory-joint clustering algorithm for time-varying channel modeling," *IEEE Transactions on Vehicular Technology*, vol. 69, no. 1, pp. 1041–1045, 2020.

[32] X. Cai, B. Peng, X. Yin, and A. P. Yuste, "Hough-transform-based cluster identification and modeling for V2V channels based on measurements," *IEEE Transactions on Vehicular Technology*, vol. 67, no. 5, pp. 3838–3852, 2018.

[33] P. J. Huber, *Robust Statistics*. Wiley-Interscience, 1981.

[34] T. Domínguez-Bolaño, J. Rodríguez-Piñeiro, J. A. García-Naya, and L. Castedo, "The GTEC 5G link-level simulator," in *1st International Workshop on Link- and System Level Simulations (IWSLS2 2016)*, Vienna, Austria, July 2016, online access: http://dx.doi.org/10.1109/IWSLS.2016.7801585.

[35] "GTEC Testbed Project," https://bitbucket.org/tomas_bolano/gtec_testbed_public.git.

[36] J. Rodríguez-Piñeiro, "Broadband wireless communication systems for high mobility scenarios," Ph.D. dissertation, University of A Coruña, 2016.

[37] T. Domínguez-Bolaño, "Design and evaluation of new waveforms for high mobility communications," Ph.D. dissertation, University of A Coruña, 2018.

[38] ETSI, "TS 136 213 V14.2.0: LTE; E-UTRA; Physical layer procedures," April 2017.

[39] B. H. Fleury, M. Tschudin, R. Heddergott, D. Dahlhaus, and K. I. Pedersen, "Channel parameter estimation in mobile radio environments using the SAGE algorithm," *IEEE J. Sel. Areas Commun.*, vol. 17, no. 3, pp. 434–450, 1999.

[40] H. Akaike, "A new look at the statistical model identification," *IEEE Trans. Autom. Control*, vol. 19, no. 6, pp. 716–723, 1974.

[41] S. Boyd, S. P. Boyd, and L. Vandenberghe, *Convex optimization*. Cambridge university press, 2004.

[42] N. Czink, C. Mecklenbrauker, and G. d. Galdo, "A novel automatic cluster tracking algorithm," in *2006 IEEE 17th International Symposium on Personal, Indoor and Mobile Radio Communications*, Sep. 2006, pp. 1–5.

[43] J. Rodríguez-Piñeiro, Z. Huang, X. Cai, T. Domínguez-Bolaño, and X. Yin, "Geometry-based MPC tracking and modeling algorithm for time-varying UAV channels," *IEEE Transactions on Wireless Communications*, vol. Early Access, 2020, online access: http://dx.doi.org/10.1109/TWC.2020.3044077.

[44] M. Hazewinkel, *Encyclopaedia of Mathematics*. Springer Netherlands.

[45] A. Papoulis and S. Pillai, *Probability, Random Variables, and Stochastic Process*. McGraw-Hill Higher Education, 2002.